PHYSICAL REVIEW A VOLUME 27, NUMBER 6 JUNE 1983

Direct radiative recombination of electrons with atomic ions: Cross sections and rate coefficients

Young Soon Kim* and R. H. Pratt
Department of Physics and Astronomy, University of Pittsburgh, Pittsburgh, Pennsylvania 15260
(Received 21 May 1982)

Simple expressions are obtained which permit systematic estimates of the rate coefficients for direct radiative recombination (DRR) of fast electrons with atomic ions of various ionic species. The analysis utilizes a set of cross sections obtained through numerical calculations combined with the use of an interpolation scheme to smoothly connect reduced cross sections (apart from normalizations) of the bremsstrahlung tip region and the low-lying DRR region. It is shown that these numerical cross sections can be reproduced by the predictions of a modified semiclassical Kramers formula with an appropriate effective charge $Z_{\rm eff}$, which is larger than the effective charge which reproduces the energy levels of the states into which capture occurs. In accord with this modified Kramers formula, the numerically obtained total cross sections are shown to scale with $Z_{\rm eff}^2/K$ for each isoelectronic sequence, and with a parameter $(n_0)_{\rm eff}$ which characterizes each isoelectronic sequence. Using these scaling properties, simple analytic expressions are obtained for recombination rate coefficients, for the rate of electron kinetic-energy loss, and for the rate of radiated power loss, assuming a classical Maxwell-Boltzmann thermal distribution of continuum electrons.

I. INTRODUCTION

Direct radiative recombination (DRR or radiative capture) is one of the important mechanisms influencing the ionization equilibria and the thermal balance in gaseous nebulas or tokamak plasma situations. To obtain the recombination rate coefficient at a given plasma temperature one performs an integration over a thermal distribution of plasma electrons to determine the thermal average of the DRR cross section weighted by the speeds of the initial electrons. Simple scaling properties of the cross sections as a function of continuum electron energy, atomic number, and/or ionic species can be useful for computation and characterization of such thermal averages as one considers plasmas of various temperatures, atomic constituents and ionic charges. The demonstration of such scalings requires a systematic and quantitative study of cross sections over a wide range of parameters. In this paper we undertake the task of finding scaling laws for DRR cross sections, allowing us to compute and characterize the relevant rate coefficients.

Lee and Pratt[1] have described a simple theoretical method for quantitative calculation of direct—radiative-recombination (DRR) cross sections which does not require separate calculation of capture into a large (in principle, infinite) number of unfilled substates; they reported results for Mo ions. The procedure involves interpolation of reduced cross sections, as a function of substate energy, between the bremsstrahlung tip region limit and DRR into low-lying states.

In this paper: (1) We extend the study of DRR cross sections to other elements (Fe and W). (2) We then use these data to examine scaling properties of the total cross sections (considered as functions of nuclear charge Z, ionic charge Z_i, and incident electron kinetic energy K, as well as the electron configuration of the initial ion). (3) Using the scaling properties of this formula, we obtain the radiative recombination rate and the rate of loss of electron kinetic energy due to the recombination process. (4) We describe a method to calculate the radiated power rate with the same simple procedures we have used to obtain other rate coefficients, and we discuss the validity of our estimate of the power-loss rates for tokamak plasmas. Natural units are used throughout this paper unless explicitly specified otherwise, i.e., $\hbar=c=m_e=1$ and $e^2=\alpha\cong 1/137.037$.

In Sec. II, we give a general overview of the problem. The DRR cross sections are discussed in Sec. III along with their scaling properties. We show that the partial cross sections can be fitted to a modified Kramers formula

$$\sigma_n = \frac{8\pi}{3\sqrt{3}} \frac{\alpha^5}{n^3} \frac{Z_{\text{eff}}^4}{K\omega} \tag{1}$$

with an appropriately chosen effective charge Z_{eff}, and that the total cross section may be written as a function of two variables: Z_{eff}^2/K and a parameter characterizing the isoelectronic sequence to which the ion belongs. Here K is the incident electron kinetic energy, ω the emitted photon energy, and n is the principal quantum number. Using the relatively simple expression and scaling features obtained in Sec. III, the various rate coefficients are estimated in Sec. IV. In the Appendix we give some details of the connection between bremsstrahlung and DRR which was utilized in obtaining the DRR cross sections on which this work has been based.

II. FEATURES AND ASSUMPTIONS OF THIS WORK

The situation we will consider is a neutral plasma of low number density ($n \lesssim 10^{15}$ cm^{-3}) and high temperature ($1 \lesssim kT < 100$ keV). In these circumstances plasma atoms are highly ionized and plasma electrons are moving rapidly, with kinetic energies K typically of order of kT (where k is the Boltzmann constant) and characterized by a thermal distribution. The density is low enough to regard the ions and electrons as free most of the time and to focus on the processes involving a single ion as though the ion were an independent isolated target. Once Kramers[2] derived the semiclassical cross-section formula for x-ray absorption in matter, the main interest (until 1960) for the study of recombination spectra and of ionization and recombination equilibrium was motivated by astrophysical concerns.[3] Subsequently, the attempts to develop laboratory fusion plasmas have given a new interest to the study of these processes.[4–8]

In recent tokamak experiments, the least highly ionized ions are the heavier impurity ions sputtered from the limiter or the wall of the container into the completely ionized hydrogen (fusion) plasma. One observes the x-ray emission from such a plasma and classifies the radiation as a continuum of bremsstrahlung and recombination radiation (dielectronic and direct), and emission line spectra of bound-bound transitions. These lines are of interest for plasma diagnostics, while the rates for the processes determine the ionic species found in the plasma and the power loss from the plasma.

Low-density plasmas can be treated as optically thin, i.e., transparent to their own radiation, and a "coronal" equilibrium is reached when the electron collisional ionization rate is balanced by the total recombination rate.[5] This implies an equilibrium in ionic species—at a given T a few characteristic degrees of ionization are present for each element—and it also implies that there is a power source of heating since energy is being lost (radiated) from the *thin* plasma. At low temperatures ($kT \lesssim 1.5$ keV for Fe-seeded hydrogen plasma,[5] for example) dielectronic recombination dominates DRR, but as the temperature increases the latter becomes relatively a more important power-loss mechanism. (However, with recent neutral-beam–injection techniques, in some plasmas charge exchange modifies the recombination rates so that dielectronic recombination remains a more important power-loss mechanism to much higher temperature, when eventually bremsstrahlung becomes the main power-loss mechanism.[9])

Here we concentrate on DRR and calculate the cross sections and the basic rate coefficients. For our DRR cross-section calculations we take the nucleus (point nuclear charge Z) of an ion (in its ground state) of ionic charge Z_i at rest. The incident continuum electron moving in the screened Coulomb field of the ion is captured into one of the infinite number of unoccupied bound states, resulting in a final ion of charge $Z_i - 1$ accompanied by emission of one photon:

$$A^{+(Z_i)} + e^- \rightarrow A^{+(Z_i-1)} + \hbar\omega \ . \tag{2}$$

(The captured electron may go through bound-bound transitions until the ion reaches its ground state, perhaps involving Auger as well as radiative emissions, or it may again be ionized by an electron or ion impact. We will not be concerned with these aftereffects here, since the most probable situation is for electrons which radiate most of their energy in the initial capture, unlike dielectronic recombination, but the need for corrections should be kept in mind.)

Further studies of DRR cross sections and rate coefficients following Seaton's work[3] are given in Refs. 10–13. We will follow the procedure Lee and Pratt[1] developed for the calculation of DRR cross sections. They numerically obtained both DRR cross sections into several low-lying unoccupied states and bremsstrahlung cross sections near the tip of the spectrum, within a single-electron model, but including relativistic, multipole, retardation, and screening effects. Considered as a function of final electron energy, the reduced cross sections $d\sigma_\kappa(\omega)/d\omega$, i.e., the cross-section density per unit energy for fixed $\kappa = (-1)^{l+j+(1/2)}(j+\frac{1}{2})$, on the negative (DRR) side of the zero final electron kinetic energy may be smoothly continued to the positive-energy cross section for the bremsstrahlung spectrum $d\sigma/d\omega$: For the reduced cross section we have

$$\left.\frac{d\sigma_\kappa(\omega)}{d(\omega/Z_i^2\alpha^2)}\right|_{\omega=\omega_n} = N^2_{\kappa,n}\sigma_{\kappa,n} ,$$

for the density of states

$$N^2_{\kappa,n} = \left.\frac{dn}{d(\epsilon/Z_i^2\alpha^2)}\right|_{\epsilon=\epsilon_{\kappa,n}} = \nu^3_{\kappa,n} + \left.\frac{d\mu_\kappa}{d(\epsilon/Z_i^2\alpha^2)}\right|_{\epsilon=\epsilon_{\kappa,n}} , \quad (3)$$

and for the photon energy

$$\omega_n = K - \epsilon_{\kappa,n} ,$$

where $\sigma_{\kappa,n}$ is the DRR cross section for capture into the (κ,n) subshell, $\epsilon_{\kappa,n}$ is the bound-state energy, μ_κ is the quantum defect, and $\nu_{\kappa n} = n - \mu_\kappa$. The DRR cross section for each n (for the given κ) is obtained from the curve at the energy-level value predicted by a smooth connection between quantum defects and low-energy continuum phase shifts. The nature of these smooth connections is discussed in the Appendix.

III. DRR CROSS SECTIONS AND THEIR SCALING PROPERTIES

In this section: (1) we present the data and predictions we have obtained for Fe and W with our numerical and interpolation methods, examining the principal quantum number n and orbital angular momentum l dependence as we vary Z, Z_i, and the incident kinetic energy K. (2) We compare the total DRR cross sections obtained in this way (a) with the values obtained from a modified Kramers formula with an effective charge $Z_{\text{eff}} = \frac{1}{2}(Z + Z_i)$ and (b) with Hahn and Rule's nonrelativistic point Coulomb values with the same Z_{eff}. (3) We discuss the scaling properties of the total cross section with Z, Z_i, and K.

Figure 1 shows the l dependence[14] of

$$\sigma_{n,l} \equiv \sum_{\kappa=-(l+1),l} \sigma_{n,\kappa}$$

for $n=5$, and (a) $K=1$ keV and (b) $K=50$ keV, for some sample Z and Z_i. Note that as Z and Z_i decrease (or some effective charge decreases) for fixed K, or as K increases for fixed charge, the peak contributions in orbital angular momentum move toward a lower l. The overall l dependence can be approximated as a Gaussian, as noted by Gau and Hahn.[15] The feature of s-wave dominance for high continuum energies is well known in photoeffect[16] and bremsstrahlung,[17] as well as the persistance of an important p-wave contribution in high-Z elements. Classically, for the calculation of Kramers[2]

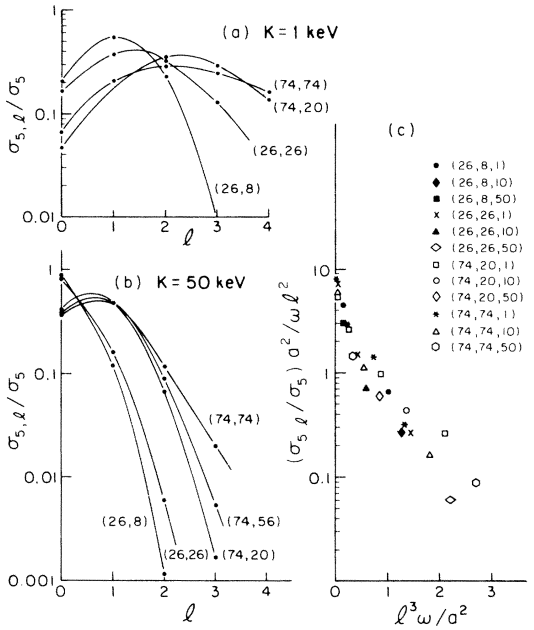

FIG. 1. l dependence of $\sigma_{n,l} = \sum_{\kappa=l,-(l+1)} \sigma_{n,\kappa}$ for the case $n=5$ for some representative (Z,Z_i), from our numerical data for $\sigma_{n,\kappa}$; (a) $K=1$ keV and (b) $K=50$ keV. We show $\sigma_{n,l}/\sigma_n$, where $\sigma_n = \sum_l \sigma_{n,l}$. As Z and Z_i decreases or as K increases, the peak contributions in orbital angular momentum move toward a lower l. (c) $(\sigma_{nl}/\sigma_n)a^2/\omega l^2$ for $n=5$ is shown as a function of $l^3\omega/a^2$, illustrating the extent to which this l dependence is given by a universal curve, independent of (Z,Z_i,K), as in the work of Kramers.

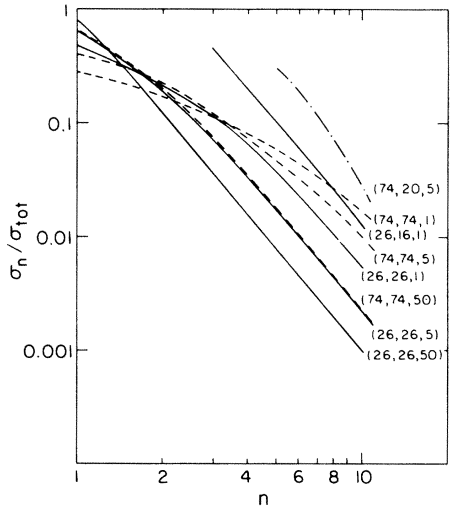

FIG. 2. n dependence of $\sigma_n = \sum_\kappa \sigma_{n,\kappa}$ for completely unfilled shells as (Z,Z_i,K) are varied. We show $\sigma_n/\sigma_{\text{tot}}$, where $\sigma_{\text{tot}} \equiv \sum_n \sigma_n$. The data show that n^{-3} scaling is valid for high n and (lower-Z, lower-Z_i, higher-K) cases reach this limit (corresponding to the straight lines decreasing by three decades for each decade of n) earlier.

TABLE I. Total DRR cross sections (in 10^{-24} cm^2) for various degrees of ionizations of Fe, Mo, and W for $1 \leq K \leq 100$ keV, with (a) our numerical methods, (b) a modified Kramers formula with $Z_{\text{eff}} = \frac{1}{2}(Z + Z_i)$ substituted for Z, and (c) predictions from Hahn and Rule's hydrogenic nonrelativistic dipole approximation method with the same effective charge. Column headings (a)—(c) relate to the above-mentioned conditions.

(Z,Z_i)	K (keV)	(a)	(b)	(c)
(26,8)	1	0.9×10^{2}	1.5×10^{2}	1.3×10^{2}
Ar-like	5	4.90	7.3	5.3
	10	1.36	1.9	1.32
	50	5.66×10^{-2}	7.6×10^{-2}	4.4×10^{-2}
	100	1.30×10^{-22}	1.9×10^{-2}	$\sim10^{-2}$
(26,16)	1	3.33×10^{2}	4.0×10^{2}	4.1×10^{2}
Ne-like	5	2.35×10^{1}	2.1×10^{1}	2.2×10^{1}
	10	6.64	5.4	6.2
	50		2.3×10^{-1}	2.2×10^{-1}
	100		5.7×10^{-2}	2.6×10^{-2}
(26,22)	1	9.98×10^{2}	1.0×10^{3}	1.1×10^{3}
Be-like	5	6.29×10^{1}	7.0×10^{1}	5.3×10^{1}
	10	1.62×10^{1}	1.9×10^{1}	1.7×10^{1}
	50	5.30×10^{-1}	9.5×10^{-1}	6.2×10^{-1}
	100		2.2×10^{-1}	0.9×10^{-1}
(26,26)	1	2.98×10^{3}	3.3×10^{3}	2.9×10^{3}
Completely	5	3.41×10^{2}	3.6×10^{2}	3.3×10^{2}
Ionized	10	1.21×10^{2}	1.2×10^{2}	1.2×10^{2}
	50	7.21	7.4	7.1
	100	1.75	2.0	1.7
(42,24)	1	1.15×10^{3}	1.5×10^{3}	0.91×10^{3}
Ar-like	5	7.57×10^{1}	9.1×10^{1}	5.6×10^{1}
	10	2.10×10^{1}	2.5×10^{1}	1.6×10^{1}
	50	0.954	1.1	0.69
	100	2.35×10^{-1}	2.7×10^{-1}	2.1×10^{-1}
(42,32)	1	2.19×10^{3}	2.5×10^{3}	2.0×10^{3}
Ne-like	5	1.78×10^{2}	1.7×10^{2}	1.5×10^{2}
	10	5.45×10^{1}	4.8×10^{1}	4.5×10^{1}
	50	2.74	2.1	2.1
	100	6.82×10^{-1}	5.4×10^{-1}	6.3×10^{-1}

(see also Landau and Lifshitz[18]) one can see that the constant Kramers energy spectrum is proportional to an integral over electron angular momentum l (incident or final become the same classically), in which l and K appear only in the combination $l^3\omega/a^2$, where $a \equiv Z_{\text{eff}}e^2$, and ω is the radiated photon energy. The dominant l of the integrand thus increases as energy decreases. Figure 1(c) shows that $(\sigma_{nl}/\sigma_n)(a^2/\omega l^2)$, where $\sigma \equiv \sum_l \sigma_n$, is indeed close to a universal function in the variable $l^3\omega/a^2$, as Kramers's work would predict; this illustrates the utility of the Kramers formula with a Z_{eff} in characterizing recombination rates.

Figure 2 shows the n dependence of $\sigma_n \equiv \sum_\kappa \sigma_{n,\kappa}$ for completely unfilled shells as Z, Z_i, and K are varied. We see that n^{-3} scaling is valid for high n, and (lower Z, lower Z_i, higher K) cases reach this limit earlier. The semiclassical Kramers formula provides a qualitative explanation, since it predicts

$$\sigma_n = \frac{8\pi}{3\sqrt{3}} \frac{\alpha^5}{n^3} \frac{Z^4}{K(K+E_n)} , \tag{4}$$

where $E_n = Z^2\alpha^2/2n^2$ is the binding energy of the level n in the point Coulomb case. If $K \gg E_n$, $\sigma_n \propto n^{-3}$.

In Table I we present total cross sections $\sigma_{\text{tot}} \equiv \sum_n \sigma_n$ calculated with our numerical methods for various degrees of ionization of Fe, Mo, and W

TABLE I. *(Continued.)*

(Z,Z_i)	K (keV)	(a)	(b)	(c)
(42,42)	1	0.999×10^{4}	1.1×10^{4}	0.9×10^{4}
Completely	5	1.28×10^{3}	1.4×10^{3}	1.1×10^{3}
Ionized	10	5.02×10^{2}	5.3×10^{2}	4.8×10^{3}
	50	4.18×10^{1}	4.2×10^{1}	3.8×10^{1}
	100	1.20×10^{1}	1.2×10^{1}	1.2×10^{1}
(74,20)	1	1.69×10^{3}	2.8×10^{3}	2.4×10^{3}
Xe-like	5	1.28×10^{2}	1.8×10^{2}	1.3×10^{2}
	10	4.06×10^{1}	4.8×10^{1}	3.3×10^{1}
	50	2.45	2.1	1.4
	100	7.45×10^{-1}	5.3×10^{-1}	3.5×10^{-1}
(74,44)	1	4.63×10^{3}	6.8×10^{3}	6.5×10^{3}
Zn-like	5	4.80×10^{2}	5.2×10^{2}	5.5×10^{2}
	10	1.57×10^{2}	1.5×10^{2}	1.6×10^{2}
	50	8.77	6.7	6.2
	100	2.40	1.7	1.3
(74,56)	1	1.1×10^{4}	1.1×10^{4}	1.1×10^{4}
Ar-like	5		9.9×10^{2}	8.9×10^{2}
	10	3.20×10^{2}	3.0×10^{2}	2.7×10^{2}
	50	1.54×10^{1}	1.5×10^{1}	1.2×10^{1}
	100	4.07	3.9	2.6
(74.64)	1		1.5×10^{4}	1.3×10^{4}
Ne-like	5	1.48×10^{3}	1.4×10^{3}	1.5×10^{3}
	10	5.14×10^{2}	4.6×10^{2}	4.8×10^{2}
	50	3.32×10^{1}	2.4×10^{1}	2.6×10^{1}
	100		6.3	6.2
(74,74)	1	4.0×10^{4}	4.1×10^{4}	3.6×10^{4}
Completely	5	5.63×10^{3}	6.0×10^{3}	4.9×10^{3}
Ionized	10	2.35×10^{3}	2.5×10^{3}	2.2×10^{3}
	50	2.65×10^{2}	2.6×10^{2}	2.2×10^{2}
	100		8.8×10^{1}	7.9×10^{1}

for $1\leq K\leq 100$ keV. For comparison we also give the predictions of Kramers's semiclassical formula with $Z_{\rm eff}=\frac{1}{2}(Z+Z_i)$ substituting for Z, and predictions from Hahn and Rule's hydrogenic nonrelativistic dipole approximation calculation with the same effective charge.[19] We note that our proposed simple formula based on Kramers's semiclassical prediction for DRR in a point $Z_{\rm eff}$ Coulomb potential

$$\sigma_n=\frac{8\pi}{3\sqrt{3}}\frac{\alpha^5 Z_{\rm eff}^4}{n^3K(K+Z_{\rm eff}^2\alpha^2/2n^2)} \tag{5}$$

approximates our numerical results fairly well in the range of energy and ionization under consideration. In fact, this simple approximation is almost as good as the more elaborate approach of Hahn and Rule with the same effective charge. For our $Z_{\rm eff}$ Kramers formula cross sections we have simply used the statistical weight W_{n_0}, the ratio between the number of unoccupied states and the total number of states in the valence shell n_0, so that

$$\sigma_{\rm tot}=W_{n_0}\sigma_{n_0}+\sum_{n\geq n_0+1}\sigma_n\ . \tag{6}$$

This simplification is one of the reasons that Hahn and Rule's nonrelativistic hydrogenic dipole approx-

imation gives a somewhat better prediction, since their calculation distinguishes the l dependence of filled and unfilled states in the valence shell. Our present choice of effective charge $Z_{\rm eff}=\frac{1}{2}(Z+Z_i)$ yields remarkable improvement over the earlier approach of Lee and Pratt, which had replaced Z with Z_i and n with the effective quantum number $\bar{\nu}=n-\bar{\mu}$, where $\bar{\mu}$ is the effective quantum defect averaged over κ for the given n. Inclusion of the quantum defect is a minor improvement in comparison with the error resulting from the choice of $Z_{\rm eff}$. This result was found to underestimate by a factor of 2–3 in the cases of partially ionized Mo ions—it should evidently be most nearly correct as one approaches complete ionization $Z=Z_i$. Other attempts[4–6,8,13] to use Kramers's formula, choosing an effective charge which produces reasonable energy levels (e.g., the choice $Z_{\rm eff}=Z-\sum_m \sigma_{nm}$, where σ_{nm} are Mayer's screening constant, giving $Z_{\rm eff}\approx Z_i<Z$) (Ref. 20), will also underestimate cross sections except for very highly ionized cases, because the wave function for a bound state is generally characterized by a larger distance than the recombination matrix element, at these high incident electron energies. (The effective charge for energy levels is even less than that for wave functions,[21] though for these unfilled outer levels of the ion the difference becomes less important.) The error in using Z_i as $Z_{\rm eff}$ is of the order $[2Z_i/(Z+Z_i)]^4$.

We can understand two major sources for the errors of the simple formula Eq. (5), as compared with our accurate numerical data in Table I. (1) $Z_{\rm eff}$ should be a function of the incident kinetic energy, and increase as the energy increases, since the important region for matrix elements is smaller at higher energies, and so in the transition the electron "sees" more of the nuclear charge. The constant $Z_{\rm eff}=\frac{1}{2}(Z+Z_i)$ is a compromise which leads to a tendency of overestimation at low energies and underestimation at high energies. (2) The weighting factors for the different angular momentum states are also dependent on incident electron kinetic energy as we see in Fig. 1. Since capture into s states dominates at very high energies, a simple statistical weight W_{n_0} for the partially filled valence shell leads to an overestimation at high energies. We observe this effect most prominently for the Be-like Fe ion, which has two $2s$ orbitals occupied and six $2p$ orbitals empty. It seems likely that with a better effective charge and with appropriate weighting factors for the different angular momentum states Eq. (5) can be used to predict DRR cross sections for a large range of energy, elements, and degrees of ionization. However, in this work we will not attempt to search for better but probably more complicated choices of $Z_{\rm eff}$ and W_{n_0}.

Now that we have a simple analytic formula which estimates cross sections σ_n reasonably well, we can study and predict the scaling properties of $\sigma_{\rm tot}$. Note that σ_n scales as

$$\sigma_n \propto \frac{1}{n^3}\frac{x^2}{1+x/2n^2},$$

with

$$x=\frac{Z_{\rm eff}^2\alpha^2}{K}\equiv\frac{a^2}{K},$$

so we may expect that the total cross sections scale with x; the only other parameter to be specified is n_0 (and W_{n_0}), or some effective (for example, noninteger) n_0 specifying initial ion configuration. Figure 3 indeed shows this scaling behavior of the numerically calculated total cross sections. Considered as a function a^2/K, all the cross sections for different Z,

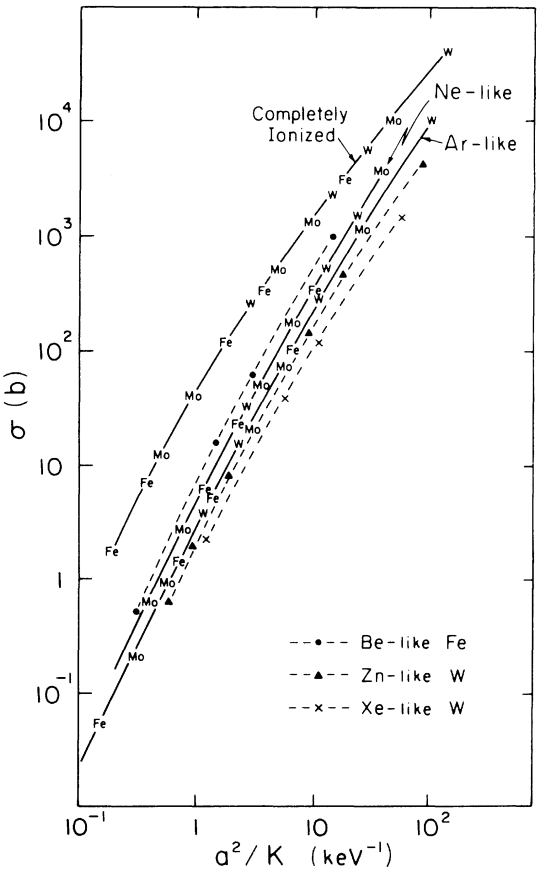

FIG. 3. Scaling of the total cross sections with a^2/K, where $a=\alpha Z_{\rm eff}=(\alpha/2)(Z+Z_i)$ and K is electron kinetic energy in keV. Cross sections for a given isoelectronic sequence fall on one curve. A series of similar curves characterizes the various isoelectronic sequences.

Z_i, and K lie on a single curve as long as they have the same initial number of electrons (same effective n_0). A different isoelectronic sequence is characterized by another but similar curve. We can predict the qualitative behavior of these curves, by replacing the summation of Eq. (6) with an integral

$$\sigma_{\rm tot} \sim \int_{(n_0)_{\rm eff}}^{\infty} \sigma_n dn = \frac{8\pi\alpha}{3\sqrt{3}} x \ln\left[1+\frac{x}{2(n_0)_{\rm eff}^2}\right], \quad (7)$$

which correctly predicts that the slope on a log-log scale approaches 1.0 as $x\to\infty$ ($K\to 0$) and approaches 2.0 as $x\to 0$ ($K\to\infty$). Here $(n_0)_{\rm eff}\sim n_0-0.3$, if n_0 is the limit on the sum and $(n_0)_{\rm eff}$ on the corresponding integral. If we have better prescriptions for a suitable effective charge $Z_{\rm eff}$ and for a suitable effective $(n_0)_{\rm eff}$, which better predict cross sections for a wide range of Z, Z_i, and K, then the curves in Fig. 3 will be better defined and smoother, and predictions for total cross sections can be made very easily by interpolation for any choice of Z, Z_i, and K.

In Fig. 4 we plot $y=\exp[3\sqrt{3}\sigma_{\rm tot}/(8\pi\alpha x)]$, as suggested by Eq. (7), as a function of $x=(a^2/K)$, with $a=\alpha Z_{\rm eff}=(\alpha/2)(Z+Z_i)$, for Ar-like, Ne-like, and completely ionized ions, using our numerical data for $\sigma_{\rm tot}$. Reasonably well-defined straight lines may be identified of the form $y=1+sx$, where a different slope s characterizes each isoelectronic sequence. According to Eq. (7) we would identify s with $[2(n_0)_{\rm eff}^2]^{-1}$, where we recall that the lower limit on a sum has been replaced by the lower limit on an integral. We have therefore achieved the parametrization of the total cross section as

$$\sigma_{\rm tot} \cong \frac{8\pi\alpha}{3\sqrt{3}} \frac{a^2}{K} \ln\left[1+s\frac{a^2}{K}\right]. \quad (8)$$

We would anticipate that this result could be made more precise with an improved choice of $Z_{\rm eff}$. With our present choice of $Z_{\rm eff}$, the $(n_0)_{\rm eff}$ are found to be 0.67, 2.8, and 3.3 for completely ionized ($s=1.1$), Ne-like ($s=0.065$), and Ar-like ($s=0.045$) ionic species, respectively. (We note that n_0 is 1, 3, and 3, respectively, in these cases.) This is in reasonable agreement with the argument $(2s)^{1/2}=(n_0)_{\rm eff}=n_0+(1-W_{n_0})-0.3$, as the characterization of $(n_0)_{\rm eff}$ for a given isoelectronic sequence. Equation (8), which expresses $\sigma_{\rm tot}$ in terms of $s\equiv[2(n_0)_{\rm eff}^2]^{-1}$ for each isoelectronic sequence, is very useful in calculating various rate coefficients, as we show in Sec. IV.

We may understand the relation between n_0 and $(n_0)_{\rm eff}$ as follows. Within our approximation we are taking equal contributions for capture into each state of a shell. With a partially filled shell the result will be between n_0 and n_0+1, and we take it as $n_0+(1-W_{n_0})$. Second, we have replaced a summation, characterized by $\sum n^{-3}$ for large n or by other powers at intermediate n, by an integration as in Eq. (7). The summations may be characterized in terms of the Rieman zeta function $\zeta(3)$ or at other integer values. Comparing the lower limits in such summations with the lower limits in corresponding integrals that yield the same results, there is a shift of the order of -0.3. Using this simple choice for $(n_0)_{\rm eff}$ together with Eq. (8) for σ, we have a simple expression for the capture cross section of *any* ion for an electron of energy K. This will lead us to corresponding simple expressions for the recombination rates of *any* ion in a plasma of temperature T.

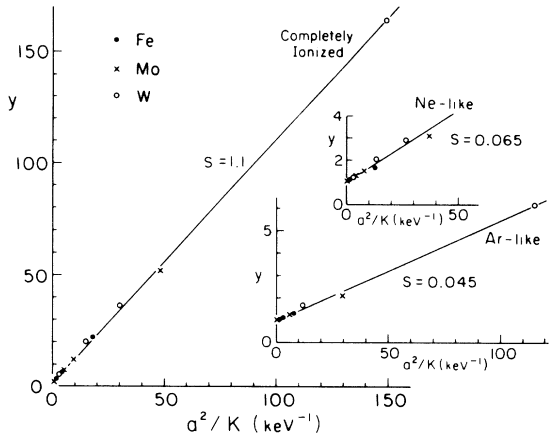

FIG. 4. Plot of $y=\exp[3\sqrt{3}\sigma_{\rm tot}/(8\pi\alpha x)]$, as suggested by Eq. (7), as a function of $x=a^2/K$ with $a=\alpha Z_{\rm eff}=(\alpha/2)(Z+Z_i)$ and K in keV, for Ar-like, Ne-like, and completely ionized ions, using our numerical data for $\sigma_{\rm tot}$. We find reasonably well-defined straight lines $y=1+sx$, where a different slope s, identified with $[2(n_0^2)_{\rm eff}]^{-1}$ according to Eqs. (7) and (8), characterizes each isoelectronic sequence.

IV. RATE COEFFICIENTS FOR RECOMBINATION, FOR LOSS OF ELECTRON KINETIC ENERGY, AND FOR RADIATED POWER LOSS

For each shell the three basic DRR plasma rate coefficients mentioned in Sec. I are given as weighted Maxwellian averages over the cross sections σ_n: (a) the recombination rate

$$\alpha_n \equiv \langle v\sigma_n\rangle = A\int_0^{\infty} p^2\sigma_n e^{-K/kT}dK, \quad (9)$$

(b) the rate of electron kinetic energy loss

$$\beta_n \equiv \langle vK\sigma_n\rangle = A\int_0^{\infty} p^2 K\sigma_n e^{-K/kT}dK, \quad (10)$$

and (c) the rate of radiated power loss

$$\gamma_n \equiv \langle v\omega_n\sigma_n \rangle = A \int_0^\infty p^2\omega_n\sigma_n e^{-K/kT} dK \ , \quad (11)$$

where $A=(2/\pi)^{1/2}(mkT)^{-3/2}$ and $\omega_n=K+E_n$, p is the incident electron momentum and v its velocity and the brackets denote the Maxwellian average. We shall assume that the temperature is not too high, so that the number of extremely relativistic electrons is very small, and consequently in calculating these averages we approximate the relativistic mass m by the rest mass and $p^2=2K+K^2\cong 2K$. The error involved will be $O(kT)$, which is 2% for $kT=10$ keV.

For the total ion DRR rate coefficients $\alpha \equiv \sum_n \alpha_n = \langle v\sigma_{\rm tot} \rangle$ and $\beta \equiv \sum_n \beta_n = \langle vK\sigma_{\rm tot} \rangle$, we use Eq. (8) to specify the total cross section $\sigma_{\rm tot}$ as a function of K and the parameter $s=[2(n_0)_{\rm eff}^2]^{-1}$ characterizing the initial ion configuration with $(n_0)_{\rm eff}$ as determined in Sec. III. From Eqs. (8) and (9),

$$\alpha = A' \int_0^\infty 2K \frac{a^2}{K} \ln\left[1+\frac{sa^2}{K}\right] e^{-K/kT} dK$$

$$= 2a^2A'kT\left[e^{+sa^2/kT}\mathrm{E}_1\left[\frac{sa^2}{kT}\right]+C+\ln\left[\frac{sa^2}{kT}\right]\right] , \quad (12)$$

where

$$A'=(2\pi/3)^{1/2}(8\alpha/3)(kT)^{-3/2} ,$$

$$C=0.5772157$$

is Euler's constant, and

$$\mathrm{E}_1(Z)=\int_Z^\infty (e^{-t}/t)dt$$

is the first exponential integral. Similarly,

$$\beta = 2a^2A' \int_0^\infty K \ln\left[1+\frac{sa^2}{K}\right] e^{-K/kT} dK$$

$$= kT\left[\alpha - 2a^4A's\, e^{+sa^2/kT}\mathrm{E}_1\left[\frac{sa^2}{kT}\right]\right] . \quad (13)$$

These expressions for α and β have required no approximations beyond those in our parametrization of $\sigma_{\rm tot}$.

Since in the power loss γ each σ_n is weighted by ω_n we cannot write the total ion rate γ in terms of the total cross section $\sigma_{\rm tot}$, but rather should insert Eq. (5) in Eq. (11) with our same $Z_{\rm eff}$ which produces reasonable cross sections, obtaining

$$\gamma = \sum_n A \int_0^\infty 2K(K+E_n) \frac{8\pi\alpha^5 Z_{\rm eff}^2}{3\sqrt{3}n^3K\left[K+\frac{\alpha^2Z_{\rm eff}^2}{2n^2}\right]} \times e^{-K/kT} dK$$

$$\cong 2A'a^4 \sum_n \frac{kT}{n^3} \cong 2A'a^4kT \int_{(n_0)_{\rm eff}}^\infty \frac{1}{n^3} dn$$

$$= 2A'a^4skT \ , \quad (14)$$

where $s\equiv[2(n_0)_{\rm eff}^2]^{-1}$ was determined previously from the total cross sections with $Z_{\rm eff}=\frac{1}{2}(Z+Z_i)$. At worst this approach gives the radiated power-loss coefficient neglecting a further factor of $[(K+a^2/2n^2)/(K+E_n)]$ for each n, while in fact it could be argued that $Z_{\rm eff}$ should only be used in the numerator of the Kramers formula, and that the denominator is precisely $K+E_n$, in which case Eq. (17) involves no further approximation. However, our data indicates that $Z_{\rm eff}$ should be used throughout the Kramers formula.

Table II gives α for Ar-like, Ne-like, and completely ionized Fe, Mo, and W at $kT=1$, 3, 10, and 30 keV. For comparison we give α calculated by Barfield[12] for Mo^{32+} and also results obtained from the hydrogenic formula

$$\alpha = 2.6\times 10^{-14}(\alpha_1+\alpha_2) \ , \quad (15)$$

where

$$\alpha_1 = Z_{\rm eff}^2\left[\frac{I_{\rm H}}{kT}\right]^{1/2} \frac{\mu}{n_0^3} \frac{I_{Z_i-1}}{kT} \times e^{I_{Z_i-1}/kT}\mathrm{E}_1\left[\frac{I_{Z_i-1}}{kT}\right] , \quad (16)$$

$$\alpha_2 = \sum_{n=n_0+1}^\infty \frac{2Z_{\rm eff}^4}{n^3}\left[\frac{I_{\rm H}}{kT}\right]^{3/2} \times \exp\left[\frac{Z_{\rm eff}^2 I_{\rm H}}{(n+\nu)^2kT}\right]\mathrm{E}_1\left[\frac{Z_{\rm eff}^2 I_{\rm H}}{n^2kT}\right]$$

$$= 2Z_{\rm eff}^2\left[\frac{I_{\rm H}}{kT}\right]^{1/2}\phi_{n_0+1}\left[\frac{Z_{\rm eff}^2 I_{\rm H}}{kT}\right] , \quad (17)$$

as used by many other authors,[4,8,13] with α in $\mathrm{cm}^3\,\mathrm{sec}^{-1}$, $I_{\rm H}=13.6$ eV, the ionization potential of hydrogen, and I_{Z_i-1} the ionization potential of the ion after recombination as tabulated in Ref. 22. The functions ϕ_{n+1} have been tabulated by Spitzer.[23] Here α_1 represents the recombination into the valence shell (of principal quantum number n_0), where μ is the number of vacant places in the valence shell and α_2 is the contribution from the ex-

TABLE II. Recombination coefficient α (in 10^{-12} cm^3/sec) for Ar-like, Ne-like, and completely ionized Fe, Mo, and W ions at electron temperature $kT=1$, 3, 10, and 30 keV. For comparison with this work, Barfield's value of α for Ne-like Mo ions at $kT=1$, 3, and 10 keV, and hydrogenic predictions with $Z_{\text{eff}}=Z_i$ and $Z_{\text{eff}}=\frac{1}{2}(Z+Z_i)$ are also given. Note the significant improvement of the hydrogenic results with the latter choice of Z_{eff}.

		Ar-like ions			Ne-like ions				Completely ionized ions	
Z	kT (keV)	This work	$Z_{\text{eff}}=Z_i$	$Z_{\text{eff}}=\frac{Z+Z_i}{2}$	This work	Barfield	$Z_{\text{eff}}=Z_i$	$Z_{\text{eff}}=\frac{Z+Z_i}{2}$	This work	Hydrogenic formula $Z=Z_i=Z_{\text{eff}}$
26	1	0.57	0.062	0.64	1.4		0.71	1.5	7.5	8.1
	3	0.14	0.016	0.19	0.42		0.20	0.45	3.1	3.5
	10	0.038	0.003 0	0.039	0.10		0.036	0.11	1.1	1.2
	30	0.0090	0.000 66	0.0079	0.027		0.0085	0.025	0.37	0.40
42	1	4.5	2.0	4.9	7.4	6.3	5.3	7.8	24	26
	3	1.5	0.62	1.6	2.6	2.2	1.8	2.8	11	12
	10	0.39	0.15	0.42	0.72	0.70	0.50	1.1	4.1	4.5
	30	0.097	0.038	0.11	0.19		0.13	0.21	1.5	1.7
74	1	31	23	33	40		35	43	94	100
	3	12	8.2	12	16		14	17	44	48
	10	3.5	2.5	3.9	4.9		4.3	5.2	18	20
	30	1.0	0.72	1.1	1.4		1.3	1.6	7.3	8.2

cited levels, considered to be hydrogenic. We give the results of this hydrogenic formula both with $Z_{\text{eff}}=Z_i$ and $Z_{\text{eff}}=\frac{1}{2}(Z+Z_i)$ in Table II. The total recombination coefficient α for Mo^{32+} obtained here agrees with Barfield's detailed calculation[12] within 20%. The hydrogenic formula with $Z_{\text{eff}}=Z_i$ clearly gives a rate coefficient too low by a factor approaching $[(Z-Z_i)/2Z]^4$ as energy becomes high, as expected, and the improvement with $Z_{\text{eff}}=(Z+Z_i)/2$ is evident. The expressions obtained here, as in Eq. (12), are appreciably simpler.

In Table III we show β and γ obtained from Eqs. (13) and (14). From these data we obtain total power-loss rate coefficients for Fe ions at $kT=1$, 3, and 10 keV as 6.2×10^{-28}, 9.4×10^{-28}, 1.5×10^{-27} W cm^3, while the results of Mertz *et al.* are 6.5×10^{-28} 8.3×10^{-28}, and 1.5×10^{-27} W cm^3.[5] (We have interpolated γ for the other Z_i of Fe, and have used the ion population distribution given in Table III of Ref. 5.)

From Tables II and III we see that, considering a fixed ionization state, the capture rates drop with increasing temperature, reflecting the fact that the basic cross section drops with increasing incident electron kinetic energy. However, the capture rates are larger for more highly ionized atoms. At these energies the increase with temperature in the number of more highly ionized atoms more than compensates for the decrease in a given rate with temperature, resulting in a total power-loss rate which *increases* with temperature, so that DRR is becoming increasingly important.[5,24]

ACKNOWLEDGMENTS

The authors wish to thank Dr. C. M. Lee and Dr. David J. Botto for help in obtaining the basic numerical cross-section data on which this discussion has been based. Dr. Lee initiated this program of work which we have developed. We are also indebted to Dr. Botto and Dr. H. K. Tseng for discussions of the accuracy and validity of the numerical data. We thank Professor R. Shakeshaft for his critical reading of the manuscript. This work was supported in part by the National Science Foundation.

APPENDIX

Apart from normalizations, low-energy wave-function shapes for a given angular momentum make a smooth transition from negative to positive energies. For any given r this smooth transition occurs (i.e., there is little change in shape going across threshold) throughout the energy interval bounded by $eV(r)$—thus with a Coulomb tail (so that there exist bound states of arbitrarily small energy)—it is guaranteed that for any finite radius r there is an interval of energies in which the change of wave-function shape goes through such a smooth transition. The corresponding reduced matrix elements (i.e., apart from normalization) of the bremsstrahlung tip region and of the DRR region, both with the same initial continuum state, can therefore also be smoothly connected for the range of energies over which wave-function shapes are changing little at the distances important for determining the ma-

TABLE III. Rate coefficients β for electron kinetic-energy loss, and the radiated power-loss rate coefficient γ for Ar-like, Ne-like, and completely ionized Fe, Mo, and W at electron temperature $kT=1$, 3, 10, and 30 keV, both in 10^{-27} W cm^3.

		Ar-like ions		Ne-like ions		Completely ionized ions	
Z	kT (keV)	β	γ	β	γ	β	γ
26	1	0.035	0.050	0.097	0.17	0.88	6.7
	3	0.015	0.029	0.070	0.097	0.93	4.3
	10	0.015	0.016	0.048	0.053	0.88	2.4
	30	0.0075	0.0092	0.030	0.031	0.74	1.3
42	1	0.69	0.71	0.69	1.6	3.0	46
	3	0.30	0.41	0.59	0.94	3.9	26
	10	0.22	0.23	0.44	0.51	4.3	14
	30	0.11	0.13	0.25	0.30	3.9	8.3
74	1	3.1	11	4.3	19	12	430
	3	3.1	6.5	4.6	11	17	250
	10	2.4	3.5	3.8	6.0	21	140
	30	1.6	2.0	2.4	3.5	22	79

trix element. This kind of connection, for example, leads to the relation between the tip region of high-energy bremsstrahlung ($\sim Z^3$) and high-energy K-shell atomic photoeffect ($\sim Z^5$), as first noted by Fano.[17] [Since at high energies the matrix elements are determined at electron Compton wavelength distances, even K-shell binding energy is smaller than eV(r) for such r.] This same connection leads to the relation between the semiclassical Kramers cross sections ($\sim Z^4$) for low incident energy DRR into a high Rydberg state and the low-energy Coulomb bremsstrahlung spectrum tip ($\sim Z^2$), as we will now qualitatively illustrate.

The electron bremsstrahlung spectrum for radiation emitted in scattering from a point Coulomb potential according to nonrelativistic quantum mechanics was obtained in dipole approximation by Sommerfeld.[25] Near the tip of the spectrum for *high incident energies* such that $2\pi\nu_i \ll 1$, where $\nu_i \equiv Z\alpha/\beta_i$ and β_i is the velocity of the initial electron ($K=\beta_i^2/2$), the result reduces to

$$\omega\frac{d\sigma}{d\omega}=\frac{64\pi}{3}\frac{Z^2}{\beta_i^2}\frac{\alpha^3\nu_i}{\omega}\propto Z^3\,, \tag{A1}$$

where ω is the photon energy radiated. At relativistic energies the final low-energy electron is predominantly in an s-wave state, while p states remain of importance in high-Z elements. For *low incident energies* $\nu_i \gg 1$ all angular momentum states contribute, and away from the soft-photon limit the Sommerfeld result reduces to the flat spectrum (valid including the tip region),

$$\omega\frac{d\sigma}{d\omega}\sim\frac{16\pi}{3\sqrt{3}}\alpha^3\frac{Z^2}{\beta_i^2}\propto Z^2\,. \tag{A2}$$

Now, the cross section at high energies for s-state photoeffect goes as Z^5, with Z^3 coming from the square of the bound-state normalizations.[26] The Sauter formula for K-shell photoeffect gives[27]

$$\sigma_{\text{photo}}^{K}=\frac{16\pi(2K)^3 2Z^5\alpha^6}{3\omega^5} \tag{A3}$$

for nonrelativistic photoelectron energies.

If we multiply the right-hand side of Eq. (A3) by $(\omega^2/p^2)=(\omega^2/2K)$ to convert it into the corresponding DRR cross section, and by the density of states $(n^3/Z^2\alpha^2)=(1/Z^2\alpha^2)$ to convert σ into $d\sigma/d\omega$, we obtain Eq. (A1), assuming $\omega\approx K$. By contrast, low-energy photoeffect cross sections for outer shells are well predicted by the Kramers formula[2]

$$\sigma_{\text{photo}}^{\text{Kramers}}=\frac{16\pi\alpha^5}{3\sqrt{3}}\frac{Z^4}{n^3\omega^3}\,. \tag{A4}$$

Again, we can obtain the same $d\sigma/d\omega$ of the low-energy bremsstrahlung spectrum Eq. (A2) by multiplying Eq. (A4) with the same factor $(\omega^2/2K)(n^3/Z^2\alpha^2)$. Note that the normalization of a low-energy Coulomb continuum s state, for example, is proportional to $Z^{1/2}$, so that reduced s-state matrix elements for small positive and small negative final energies (factoring out normalizations) are proportional to $Z^{1/2}$ for low initial energies and to Z for high initial energies.

Figure 5(a) schematically illustrates the connec-

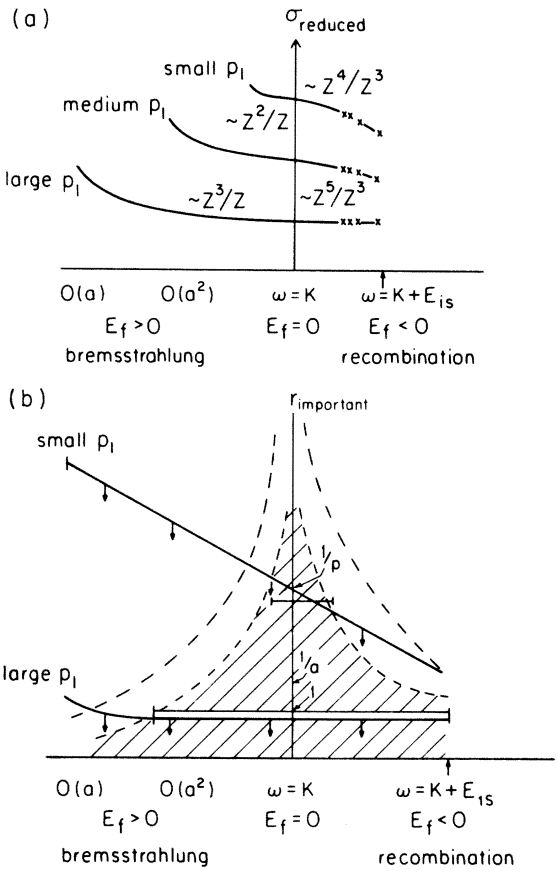

FIG. 5. Schematic diagrams. (a) Illustration of the smooth connections between the reduced cross sections of positive and negative final electron kinetic-energy regions. While these reduced cross sections are independent of final-state angular momentum, the cross sections and normalization Z dependences shown are for a final s state. (b) Illustration of important regions of matrix elements for high and low incident electron energies as a function of final electron energy. Downward arrows indicate that the important distances are *below* each solid curve. Shaded area indicates the ranges of r where the low-energy wave-function shapes are similar, and the outer pair of the dashed curves represents the typical distance which determines a bound state of energy $|E|$. Horizontal barred lines indicate, for the two choices of p_1, the ranges of E_f in which the reduced cross sections will be similar.

tion between the reduced cross sections for positive and negative final electron kinetic energies. We also schematically show in Fig. 5(b) the important regions of matrix elements for high and low incident electron energies as a function of final electron energy. The shaded area indicates the range of energy where, for each given r, the low-energy wavefunction shapes may be considered similar and largely independent of energy. The two curves labeled as small P_1 and large P_1 represent, for two definite initial electron energies, the maximum important distance for the matrix element as a function of final electron kinetic energy. The portion of such a curve lying within the shaded region therefore represents the range of final electron kinetic energies for which the reduced matrix element will be only a slowly varying function of the final energy. Note that the important distances at which matrix elements are determined are smaller for higher incident electron energies. Further, note that the effective charge the electron will "see" in the transition is typically larger than either the ionic charge or the effective charge which produces accurate energy levels. We also show in Fig. 5(b) the typical distance which determines a bound state of energy $|E|$; particularly for high incident energies this distance will be larger than the distance at which the matrix element is determined.

---

*Present address: Department of Physics, University of Southern California, Los Angeles, California 90007.

[1]C. M. Lee and R. H. Pratt, Phys. Rev. A 12, 1825 (1975); 14, 990 (1976).

[2]H. A. Kramers, Philos. Mag. 46, 836 (1923).

[3]M. J. Seaton, Mon. Not. R. Astron. Soc. 119, 82 (1959). For further discussion and additional references see Wallace H. Tucker, *Radiation Processes in Astrophysics*, (MIT University Press, Cambridge, Mass., 1975), pp. 218–223.

[4]S. von Goeler, W. Stodiek, H. Eubank, H. Fishman, S. Grebenshchikov, and E. Hinnov, Nucl. Fusion 15, 301 (1975).

[5]A. L. Merts, Robert D. Cowan, and N. H. Magee, Jr., Los Alamos Scientific Laboratory Informal Report No. LA-6220-MS (unpublished).

[6]D. E. Post, R. V. Jensen, C. B. Tarter, W. H. Gradberger, and W. A. Lokke, At. Data Nucl. Data Tables 20, 397 (1977).

[7]V. I. Gervids and V. I. Kogan, Zh. Eksp. Teor. Fiz. 69, 647 (1975) [Sov. Phys.—JETP 21, 329 (1975)].

[8]C. Breton, C. DeMichelis, M. Mattioli, Nucl. Fusion 16, 891 (1976); J. Quant. Spectrosc. Radiat. Transfer 19, 367 (1978); C. Breton, C. DeMichelis, M. Finkenthal, and M. Mattioli, Phys. Rev. Lett. 41, 110 (1978).

[9]S. Suckewer, E. Hinnov, M. Bitter, R. Hulse, and D. Post, Phys. Rev. A 22, 725 (1980).

[10]C. B. Tarter, Astrophys. J. 168, 313 (1971); 181, 607 (1973).

[11]S. N. V. Aldrovandi and D. Pèquignot, Astron. Astrophys. 25, 137 (1973).

[12]W. D. Barfield, J. Phys. B 13, 931 (1980); see also the reference therein.

[13]Christopher Bottcher, in *Atomic and Molecular Processes in Controlled Thermonuclear Fusion*, edited by M. R. C. McDowell and A. M. Ferendeci, NATO Advanced Study Institutes Series, Series B. Volume 53 (Plenum, New York, 1980).

[14]For a discussion of the branching ratios of cross sections to fine-structure split states (same l, different j or κ) see Akiva Ron, Young Soon Kim, and R. H. Pratt, Phys. Rev. A 24, (1981).

[15]J. N. Gau and Y. Hahn, Phys. Lett. 68A, 197 (1978).

[16]R. H. Pratt, Phys. Rev. 117, 1017 (1960); 119, 1619 (1960).

[17]U. Fano, Phys. Rev. 116, 1156 (1959); K. W. McVoy and U. Fano, *ibid.* 116, 1168 (1959); U. Fano, H. W. Koch, and J. W. Motz, *ibid.* 112, 1679 (1958); R. J. Jabbur and R. H. Pratt, *ibid.* 129, 184 (1963).

[18]L. Landau and E. Lifshitz, *The Classical Theory of Fields* (Addison-Wesley, Reading, Mass., 1951), pp. 197–202.

[19]Y. Hahn and D. W. Rule, J. Phys. B 10, 2689 (1977).

[20]See, for example, W. A. Lokke, W. H. Grasberger, Lawrence Livermore Laboratory Report No. UCRL-52276 (unpublished).

[21]John C. Slater, *Qunatum Theory of Atomic Structure* (McGraw-Hill, New York, 1960), Vol. 1, pp. 203 and 228.

[22]D. A. Carlson *et al.*, At. Data 2, 63 (1970).

[23]Lyman Spitzer, Jr., Astrophys. J. 107, 6 (1948).

[24]Recently, a large recombination edge corresponding to recombination of electrons with hydrogenlike argon ions into the ground state of the heliumlike charge state was observed in a colder region of the tokamak plasma and attributed to a departure from coronal equilibrium. At the same time this provided an experimental confirmation of DRR. See K. Brau *et al.*, Phys. Rev. A 22, 2769 (1980).

[25]A. Sommerfeld, Ann. Phys. (Leipzig) 11, 257 (1931).

[26]R. H. Pratt, A. Ron, and H. K. Tseng, Rev. Mod. Phys. 45, 273 (1973).

[27]Hans A. Bethe and Edwin E. Salpeter, *Quantum Mechanics of One- and Two-Electron Atoms* (Plenum, New York, 1977), p. 313 (for the cross section per electron).